Ninth International Conference on Computational Fluid Dynamics (ICCFD9), Istanbul, Turkey, July 11-15, 2016

ICCFD9-xxxx

Optimal Flow Actuation for Separation Control and Noise Minimization

Beckett Y. Zhou[1], Tim Albring[1], Nicolas R. Gauger[1]

[1] Chair for Scientific Computing, TU Kaiserslautern, 67663 Kaiserslautern, Germany

Corresponding author: yuxiang.zhou@scicomp.uni-kl.de

Abstract: We present an optimal flow control framework in which algorithmic differentiation (AD) is applied to the open-source multi-physics solver SU2 to obtain control sensitivities. An AD-based consistent discrete adjoint solver is developed which directly inherits the convergence properties of the primal flow solver due to the differentiation of the entire nonlinear fixed-point iterator. The resultant framework is applied to the lift maximization and noise minimization case of a wing-flap configuration.

Keywords: Flow Control, Computational Fluid Dynamics, Optimization, Aeroacoustics.

1 Introduction

One cannot overstate the tremendous technological importance of the ability to manipulate complex, unsteady flows by tailoring it from one state into a more desired state. Consequently, decades of effort by many researchers have been devoted to the field of active flow control (AFC). As shown by the rich body of past research, AFC promises enormous benefits including reduced fuel consumption (and increased range), noise reduction, and reduced system weight. AFC technologies have been proposed for a wide range of applications such as separation control on aircraft high-lift systems for lift enhancement to enable short landing and takeoff, modification of wake structures behind large transport trucks for drag reduction, and noise suppression on wind turbine and engine fan blades. A good review of various AFC methodologies is presented by Gad el Hak in [1].

Despite decades of research effort, a number of limitations have prevented AFC from being widely used in real life applications. First and foremost, the optimal set of flow actuation parameters are not typically known a priori for most complex 3D flows. In addition, large number of actuators lead to large numbers of actuation parameters to be determined. To that end, adjoint-based optimization coupled with a high-fidelity flow solver can be used to search for the optimal parameters at a fixed computational cost, independent of the number of actuation parameters. A recent work involving optimal flow control of a large-scale 3D high-lift configuration using a discrete adjoint approach is presented by Nemili et al. [2]. Another bottleneck impeding the use of AFC is its robustness in real-time operations under uncertain operating conditions. Therefore the 'real-life' challenges call for the development of a 'real-time' strategy for the control of various unsteady phenomena. To that end, the control sensitivity information attainable from the adjoint-based methods will prove to be extremely useful in the off-line construction of the requisite surrogate model and hence greatly enhance the accuracy of an online controller such as model predictive control.

In this paper, we present the development of an optimal AFC framework using an AD-based discrete adjoint approach, on an open source multi-physics suite SU2 [3] for applications to separation control and noise reduction problems. In particular, we couple the current AFC framework with our previous work on aeroacoustic optimization [4], also developed on the basis of SU2. This allows us to investigate the potentially competing design objectives by performing aerodynamic and aeroacoustic optimizations. Furthremore, it

enables us to perform separation control using far-field noise as a constraint or vice versa in the near future. The remainder of the paper is organized as follows. In Section 2, the unsteady SU2 solver including the active flow control implementation and a coupled CFD-CAA model using a permeable surface Ffowcs Williams-Hawkings (FW-H) approach as well as the optimization framework based on discrete adjoint and AD are presented. The optimal flow control framework thus established are applied to the lift maximization and noise minimization problem of a wing-flap geometry in Section 3. The conclusion and outlook for future work are outlined in Section 4.

2 Optimal Active Flow Control Framework

2.1 Unsteady Multi-Physics Solver SU2

The Stanford University Unstructured (SU2) open source software suite was specifically developed for solving problems governed by partial differential equations (PDEs) and PDE-constrained optimization problems. It was developed with the aerodynamic shape optimization problems in mind. Therefore the suite is centered around a RANS solver capable of simulating compressible, turbulent flows in aerospace applications. The governing equations are spatially discretized using the finite volume method, on unstructured meshes. A number of convective fluxes discretization schemes have been implemented, such as the Jameson-Schimdt-Turkel (JST) scheme and the upwind Roe scheme. The turbulence can be either modeled by the Spalart-Allmaras(S-A) model or the Menter Shear Stress Transport (SST) Model. For unsteady flows, a dual time-stepping method can be used to obtain time-accurate solutions. SU2 suite has recently seen extensions in the multi-disciplinary setting such as the inclusion of a wave equation solver and a structural solver, making it well-suited for the unsteady multi-physics problems considered in this work. For numerical details on the SU2 solver, please refer to the published work of Economon et al. of the SU2 team [3].

2.2 Coupled CFD-CAA Noise Prediction using a Permeable Surface Ffowcs Williams-Hawkings Approach

For turbulent flows at low Mach numbers, direct computations of far-field noise is computationally prohibitive [5]. A common way to perform far-field noise prediction is then to adopt a hybrid CFD-CAA approach in which the near-field noise source region is computed using a high-fidelity CFD model and then propagated to the far-field using a computationally cheaper wave equation like CAA model.

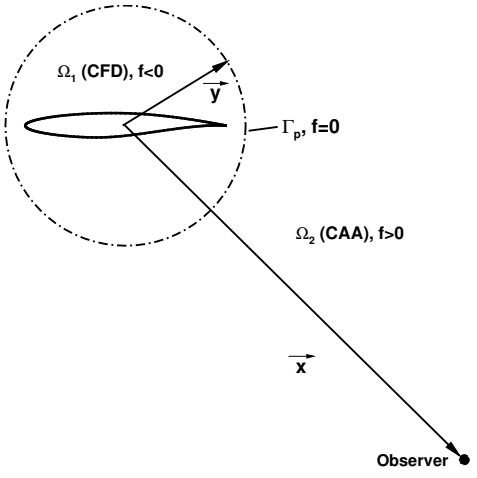

Figure 1: Permeable control surface Γ_p separating the CFD and CAA domains

To that end, integral methods based on the Kirchhoff or Ffowcs Williams-Hawkings (FW-H) formulations offer a more efficient approach for calculating acoustic pressure at arbitrary observer locations by performing boundary integrals once the appropriate field data is known. In this manner, the radiated noise from a complex system can be calculated given the near-field flow data supplied by a CFD solution. In this work, noise prediction is performed using such hybrid approach coupling the SU2 URANS solver with a propagation model based on a frequency-domain permeable surface Ffowcs Williams-Hawkings approach [6]. For the sake of keeping this paper self-contained, we briefly describe the hybrid method here. The details of formulation, implementation and validation of the hybrid CFD-CAA solver can be found in our previous publication [4].

The permeable FW-H formulation distinguishes itself from its original formulation in that it allows fluid to flow through the discontinuity surface. Consequently, one can define any arbitrary smooth sur-

rounding surface Γ_p around the aerodynamic body S where details of the flow field are extracted and the noise source can be propagated to the far-field. A schematic of such permeable surface is shown on Figure 1. The fluid domain is therefore divided into two regions – the near-field CFD region Ω_1 and far-field CAA region Ω_2. Further, we define the shape of Γ_p by a function, $f = 0$, such that $f < 0$ inside the control surface and $f > 0$ outside the control surface. The CAA module is implemented and interfaced with the remainder of the SU2 suite as follows: an unsteady flow simulation is first performed. At every time step, the primitive flow variables at each point on the permeable surface are extracted in order to compute the noise source terms. At the end of the CFD simulation, the respective mean values are subtracted from source terms as they correspond to zero frequency components which do not generate any noise. Due to the fact that it is practically impossible to ensure perfectly periodic flow data from most CFD calculations, a Hanning-type windowing function is applied to the zero-mean source terms to prevent spectral leakage [6]. The windowed source terms are then Fourier transformed using fast Fourier transformation (FFT). The pressure fluctuation in frequency domain can be computed by numerically integrating along the permeable surface, for each observer location $\vec{\mathbf{x}}$ and frequency ω. Finally, pressure fluctuation $p'(\vec{\mathbf{x}}, t)$ in time domain can be recovered using an inverse FFT.

2.3 Flow Actuation Formulation

The active flow control is realized using N actuation slits of synthetic jets with periodic blowing, which are modeled as time-dependent in-flow boundary conditions on the aerodynamic surface. In particular, the actuation velocity $\vec{V}_{in}^{i}$ prescribed at the i-th actuation slot is given by a 'clipped' sinusoidal function

$$\vec{V}_{in}^{i} = max\{0, V_A^i sin(2\pi f^i(t - \phi^i))\hat{v}^i\}, \qquad i = 1, ..., N \tag{1}$$

where V_A^i, f^i and ϕ^i are the actuation amplitude, frequency and phase shift at each slot respectively and $\hat{v}^i$ is the unit vector in the direction of the actuation velocity. Note that the actuation velocity is clipped at a minimum value of zero in order to simplify the numerical boundary condition necessary for this work. The same approach is used by Nielsen and Jones [7].

2.4 AD-based Unsteady Discrete Adjoint Framework

The implementation of the discrete adjoint formulation in this work is eased by the use of automatic differentiation (AD) [8], eliminating the error-prone hand-differentiation of the discretized equations. AD was developed based on the observation that any simulation code, regardless of its complexity is merely a sequence of elementary operations whose differentiation rules are well known. Therefore, by successive applications of the chain-rule through the computer program, it is possible to compute both the simulation output and its derivative with respect to prescribed design variables simultaneously. A remarkable feature of AD, owing to its construction, is that it does not incur any truncation errors compared to the traditional finite difference method. In particular, the derivatives are accurate to machine accuracy. This is a very attractive characteristic of AD, since accurate evaluation of the gradient requires exact differentiation of the fixed point iterator G^n as evidenced by Equations 15 and 16 in the following discussion.

In the following we present our AD-based unsteady discrete adjoint framework in the particular context of active flow control, using a simple system of PDEs as an example. Consider a system of semi-discretized PDEs as follows:

$$\frac{dU}{dt} + R(U) \quad = \quad 0 \tag{2}$$

where U is the spatially discretized state vector and $R(U)$ is the discrete spatial residual vector. For the sake of illustration, we assume the second-order backward difference is used for time discretization, which leads to the following system of equations:

$$R^*(U^n) \quad = \quad \frac{3}{2\Delta t}U^n + R(U^n) - \frac{2}{\Delta t}U^{n-1} + \frac{1}{2\Delta t}U^{n-2} = 0, \qquad n = 1, \ldots, N \tag{3}$$

The application of dual-time stepping method then solves the following problem through a fictitious time τ

to converge to a steady state solution in (3):

$$\frac{dU^n}{d\tau} + R^*(U^n) = 0 \tag{4}$$

Further assume the implicit Euler method is used to time march the above equation to steady state.

$$U^n_{p+1} - U^n_p + \Delta\tau R^*(U^n_{p+1}) = 0, \qquad p = 1, \ldots, M \tag{5}$$

The resultant nonlinear system can be linearized around U^n_p to solve for the state U^n_{p+1}

$$U^n_{p+1} - U^n_p + \Delta\tau \left[R^*(U^n_p) + \left.\frac{\partial R^*}{\partial U}\right|^n_p (U^n_{p+1} - U^n_p) \right] = 0, \qquad p = 1, \ldots, M \tag{6}$$

This can be written in the form of a fixed-point iteration:

$$U^n_{p+1} = G^n(U^n_p, U^{n-1}, U^{n-2}), \qquad p = 1, \ldots, M, \quad n = 1, \ldots, N \tag{7}$$

where G^n represents an iteration of the pseudo time stepping. U^{n-1} and U^{n-2} are the converged state vectors at time iterations $n-1$ and $n-2$ respectively. The fixed point iteration converges to the numerical solution U^n:

$$U^n = G^n(U^n, U^{n-1}, U^{n-2}), \qquad n = 1, \ldots, N \tag{8}$$

The discrete optimization problem can then be posed as:

$$\min_{\alpha} \quad J = f(U^{N_*}, \ldots, U^N, \alpha) \tag{9}$$

$$\text{subject to} \quad U^n = G^n(U^n, U^{n-1}, U^{n-2}, \alpha), \qquad n = 1, \ldots, N \tag{10}$$

where α is the vector of active flow control variables and the objective function J is evaluated between $N_* \leq n \leq N$. One can express the Lagrangian associated with the above constrained optimization problem as follows:

$$L = f(U^{N_*}, \ldots, U^N, \alpha) - \sum_{n=1}^{N} [(\bar{U}^n)^T (U^n - G^n(U^n, U^{n-1}, U^{n-2}, \alpha))] \tag{11}$$

where $\bar{U}^n$ is the adjoint state vector at time level n. The first order optimality conditions are given by:

$$\frac{\partial L}{\partial \bar{U}^n} = 0, \quad n = 1, \ldots, N \qquad \text{(State equations)} \tag{12}$$

$$\frac{\partial L}{\partial U^n} = 0, \quad n = 1, \ldots, N \qquad \text{(Adjoint equations)} \tag{13}$$

$$\frac{\partial L}{\partial \alpha} = 0, \qquad \text{(Control equation)} \tag{14}$$

From (13), the unsteady discrete adjoint equations can be derived in the fixed point form as:

$$\bar{U}^n_{i+1} = \left(\frac{\partial G^n}{\partial U^n}\right)^T \bar{U}^n_i + \left(\frac{\partial G^{n+1}}{\partial U^n}\right)^T \bar{U}^{n+1} + \left(\frac{\partial G^{n+2}}{\partial U^n}\right)^T \bar{U}^{n+2} + \left(\frac{\partial f}{\partial U^n}\right)^T, \; n = N, \ldots, 1 \tag{15}$$

where $\bar{U}^{n+1}$ and $\bar{U}^{n+2}$ are converged adjoint state vectors at time levels $n+1$ and $n+2$. The unsteady adjoint equations above are solved backward in time. At each time level n we iterate through inner iteration i until we have converged to $\bar{U}^n$. The highlighted terms here are evaluated in reverse mode AD at each iteration. To do so, reverse accumulation [8] is performed at the beginning of each time level n to store the computational graph by evaluating G using converged state solution U_n. Then each inner iteration i proceeds by re-evaulating the tape using the updated adjoint vector $\bar{U}^n_i$, giving the highlighted terms. This

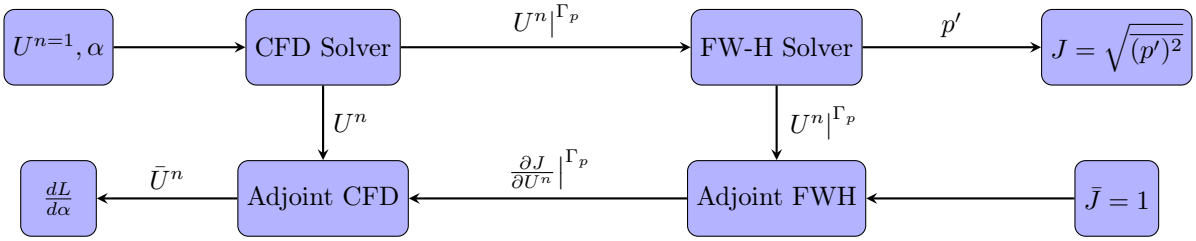

Figure 2: Computational chain of the coupled CFD-FWH noise prediction and optimization framework

continues within each time level n until the adjoint vector has converged to $\bar{U}^n$. Note that $\frac{\partial f}{\partial U^n} = 0$ for $n < N_*$. The sensitivity gradient can then be computed from the adjoint solutions:

$$\frac{dL}{d\alpha} = \frac{\partial f}{\partial \alpha} + \sum_{n=1}^{N} \left(\left(\bar{U}^n\right)^T \frac{\partial G^n}{\partial \alpha} \right) \tag{16}$$

The computational chain for the coupled CFD-FWH noise prediction and noise-adjoint framework is outlined on Figure 2. In the primal phase, unsteady flow field U^n is realized at each time step n by the SU2 CFD solver via Equation 7. $U^n|^{\Gamma_p}$ denotes the conservative flow variables at time step n extracted from the FW-H surface Γ_p which are then passed to the FW-H solver for far-field noise computation. In the adjoint phase, $\frac{\partial J}{\partial U^n}|^{\Gamma_p}$ denotes the sensitivity of the noise objective with respect to conservative flow variables evaluated Γ_p by the adjoint FW-H solver using $U^n|^{\Gamma_p}$, which is accumulated to the fixed-point iteration for the adjoint flow variables $\bar{U}^n$ in the adjoint CFD solver (Equation 15).

Typically AD is introduced based on the observation that every code is merely a sequence of elementary functions that depend on one or two variables. Although this assumption leads to an intuitive approach for the implementation it is rather inefficient, as we have to store information for each single operation. Another approach is to apply AD on the statement-level. Here we only need to store information for each statement, independent of the number of operations involved. An efficient way to compute the partial derivatives of statements is the use of the Expression Template technique [9]. The overloaded operators no longer return the (computationally expensive) result of an expression, but a small temporary object that acts as a placeholder for this particular expression. Using this objects we can build an internal representation of each expression to directly compute and store the required derivative information. These overloaded operators and a corresponding datatype are provided by the C++ library CoDiPack [10]. A simple replacement of the usual double datatype inside of SU2 with this new AD type enables the rapid development of adjoint solvers for arbitrary state equations and physical models – the adjoint solver can be automatically updated with primal code modification and one can easily define any objective function from any state variable. This is an extremely attractive characteristic for unsteady optimization problems in the multidisciplinary setting using a suite of multi-physics solvers where the objective function may be different depending on the type of problems being addressed. To alleviate the high-memory requirements and for the general improvement of performance we apply preccumulation strategies and an explicit treatment of the linear solvers. Furthermore, the adjoint solver is automatically parallelized using the AdjointMPI library.

3 Optimization Results

3.1 Validation of Control Sensitivities

To validate the control sensitivities with respect to both aerodynamic and aeroacoustic design objectives, we apply active flow actuation to the canonical test case of controlling the laminar ($Re = 100$) vortex shedding of a 2D circular cylinder at $M_\infty = 0.2$. Two actuation orifices are placed on the pressure recovery side of the cylinder, located at $\pm 75°$ from the rear stagnation point. The control variables are V_A^i, f^i, and ϕ^i (actuation flow angle), on both slits. The in-flow velocity at each slit is assumed fixed normal to the

slit surface. The baseline actuation for which the control sensitivities are evaluated are set to be in-phase ($\phi^1 = \phi^2 = 0$) periodic blowing with the same actuation amplitude of $V_A^1 = V_A^2 = 0.1U_\infty$ and frequency of $f^1 = f^2 = 1.0Hz$.

First, the control sensitivities with respect to the drag objective function ($J = \overline{C}_d$) are computed using the adjoint-mode AD over 100 time steps and compared with second order centered difference (FD) results computed with a step size of $\delta = 10^{-6}$. As shown on Table 1, adjoint sensitivities attain excellent accuracy. The disagreement in the phase-shift sensitivity is likely due to the loss of accuracy of the finite difference result at such small sensitivity value.

Next, the control sensitivities with respect to the noise objective function ($J = \sqrt{\overline{(p')^2}}$) is computed using adjoint-mode AD and FD, on the same set of control parameters, over 100 time steps. As shown on Table 2, the agreement is again excellent.

Consequently, we conclude that the control parameter sensitivities are validated to very good accuracy and therefore can be used to perform active flow controls for aerodynamic and aeroacoustic objectives.

Slit 1	Finite Difference (FD)	Adjoint Mode AD
V_A^1	0.008009100049	0.008008918670
ω^1	-0.003363247458	-0.003363435599
ϕ^1	-5.41051647928e-07	-5.40633964356e-07

Table 1: Control parameter sensitivities at Slit 1 with respect to the drag objective function ($J = \overline{C}_d$) using 2nd order FD ($\delta = 10^{-6}$) and adjoint mode of AD, over 100 time steps

Slit 1	Finite Difference (FD)	Adjoint Mode AD
V_A^1	5.47800027e-07	5.47836945e-07
ω^1	2.23900542e-04	2.23972586e-04
ϕ^1	-2.27060041e-04	-2.27071110e-04

Table 2: Control parameter sensitivities at Slit 1 with respect to the noise objective function ($J = \sqrt{\overline{(p')^2}}$) using 2nd order FD ($\delta = 10^{-6}$) and adjoint mode of AD, over 100 time steps

3.2 Optimal Flow Actuation for a Wing-Flap Configuration

In this subsection, we apply the optimal flow control framework outlined in Section 2 on the NLR7301 wing-flap geometry to perform lift maximization and noise minimization. The freestream Mach number is $M_\infty = 0.2$. Laminar flow is assumed with $Re = 800$. The wing-flap configuration is set at an angle of attack of 15 degrees, with the flap deflected at 30 degrees. Under such post-stall condition, the configuration suffers massive flow separation on both the wing and flap suction sides, leading to a marked loss of lift. In addition, vortices periodically shed from the wing and the flap give rise to strong tonal noise.

The role of active flow control is to delay and reduce the extend of flow separation in order to enhance the lift characteristics of the configuration, as well as suppressing the tonal noise generation. To that end, we place a total of 18 actuation slits on the wing-flap configuration. 10 slits are installed on the suction side of the main wing, evenly spaced between the 30% chord and the trailing edge, as shown on Figure 3(a). 8 slits are installed on the suction side of the flap, evenly spaced between the 25% flap chord and the flap trailing edge, as shown on Figure 3(b). On the main wing, each slit surface span 1.5% of the main wing surface while each slit on the flap span 3.0% of the flap surface.

An unstructured O-mesh is used for this geometry with 39,000 triangular elements and refinement on each of the 18 slit surfaces. The permeable FW-H surface is a circle of diameter $D_{FWH} = 2.0$ concentric to geometric center of the wing-flap configuration. The unsteady CFD solution is computed using the second-order dual time-stepping method with a time step of $\Delta t = 0.001$.

Both lift maximization and noise minimization are performed. The lift maximization is performed over 800 time steps with the optimization window defined to be the last 300 time steps which approximately correspond to 6 periods of vortex shedding. To further ensure that the unsteady flow has settled into a

periodic steady state (due to the inherent assumption of the 2D frequency-domain FW-H formulation), the noise minimization is performed over 1600 time steps with the optimization window defined to be the last 512 time steps. Furthermore, for the noise minimization case, the observation locations are placed equidistantly along a line $20c_{wing}$ below the cylinder at $(-20c_{wing}, -20c_{wing})$, $(0, -20c_{wing})$, and $(20c_{wing}, 20c_{wing})$. To ensure physically realizable actuation parameters, the velocity magnitude V_A^i and actuation frequency f^i are constrained to $-10m/s \leq V_A^i \leq 10m/s$ and $f^i \leq 50Hz$ for all 18 slits in both optimizations. The baseline actuation parameters are set to be in-phase ($\phi^1 = \phi^2 = 0$) periodic blowing with the same actuation amplitude of $V_A^1 = V_A^2 = 1m/s$ and frequency of $f^1 = f^2 = 1.0Hz$.

The corresponding convergence histories for the two optimization cases are shown on Figure 4 (a) and (b). Note that while approximately 550 additional lift counts are attained by optimal flow actuation in the lift maximization case, little noise reduction is achieved. This is likely due to the fact that these actuators, while periodically injecting fluid into the flow above the surface, generate noise themselves. The advantage of optimal flow actuation is demonstrated on Figure 5 – while the baseline actuation parameters improve the time-averaged lift by 761 counts from the un-actuated case, the optimal actuation parameters obtains an *additional* 550 lift counts from the baseline performance.

Figure 6 to 8 compare the optimal actuation parameters obtained by the lift maximization and noise minimization at all 18 slits. It appears that to maximize lift, the strength of actuation input (V_A^i on Figure 6) required is at least an order of magnitude stronger than that is necessary in the noise minimized case, likely due to the need to modify the massively separated flow structure immediately adjacent to the aerodynamic surface. Note that Figure 6(a) also shows the optimal actuations used on the wing is at least three times stronger than those on the flap. This is not surprising as at the angel of attack of 15 degrees, the flow over the main wing is largely separated – more lift augmentation can be achieved by flow actuation on the wing than the flap. Figure 7 shows that the actuators need to be operating at much higher frequency for noise reduction purpose than for lift enhancement. This is due to the fact that to improve lift, the actuation frequency is typically set at the shedding frequency which is much lower than the frequency necessary to suppress noise generation – a phenomenon containing high frequency components due to the complex interactions of vortices shedding from both the wing and the flap. Figure 8 shows that the phase disparities between various slits are much larger in the lift-maximized case than the noise minimized case.

Finally, it must be noted that the aerodynamic and aeroacoustic design objectives are in direct competition with each other in this case. As shown by the red off-diagonal entries on Table 3, when the set of optimal actuation parameters obtained in the lift-maximized case is used, it leads to an amplification of far-field noise. Conversely, the noise-minimized set of control parameters results in a significant loss of lift even from the baseline performance.

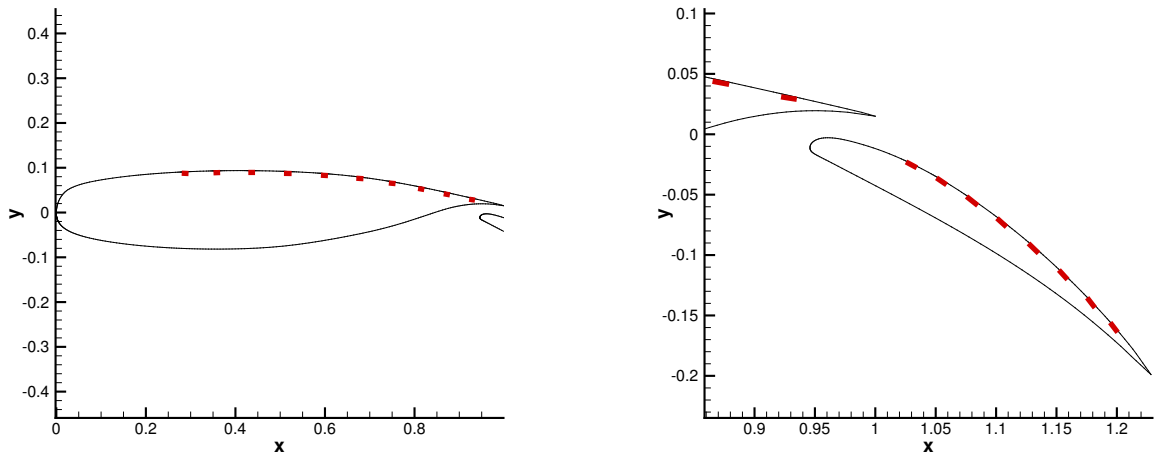

(a) 10 slits on the wing

(b) 8 slits on the flap

Figure 3: 18 actuation slits on the wing and flap suction side

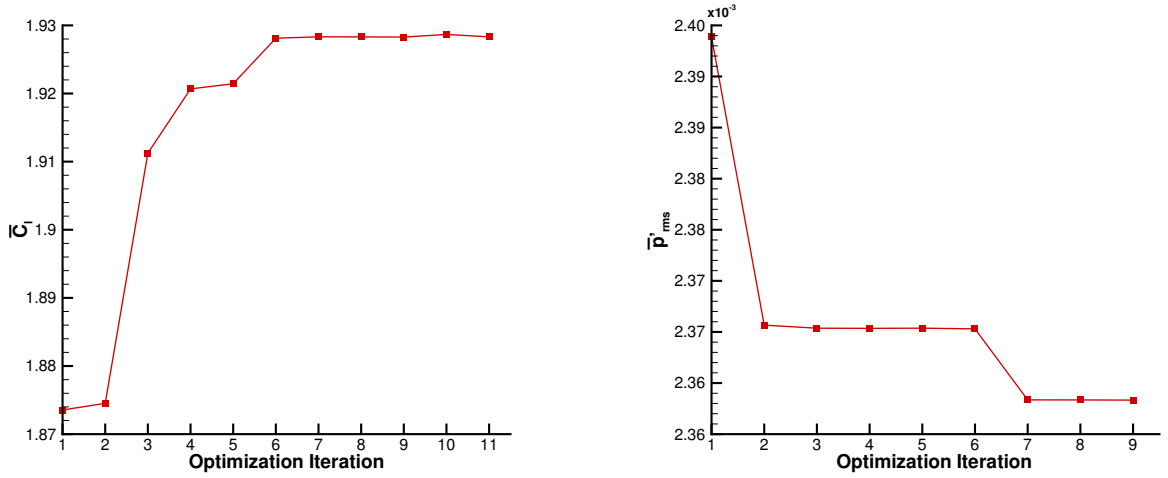

(a) Lift Maximization

(b) Noise Minimization

Figure 4: Optimization history of the lift maximization and noise minimization cases of the NLR7301 wing-flap geometry

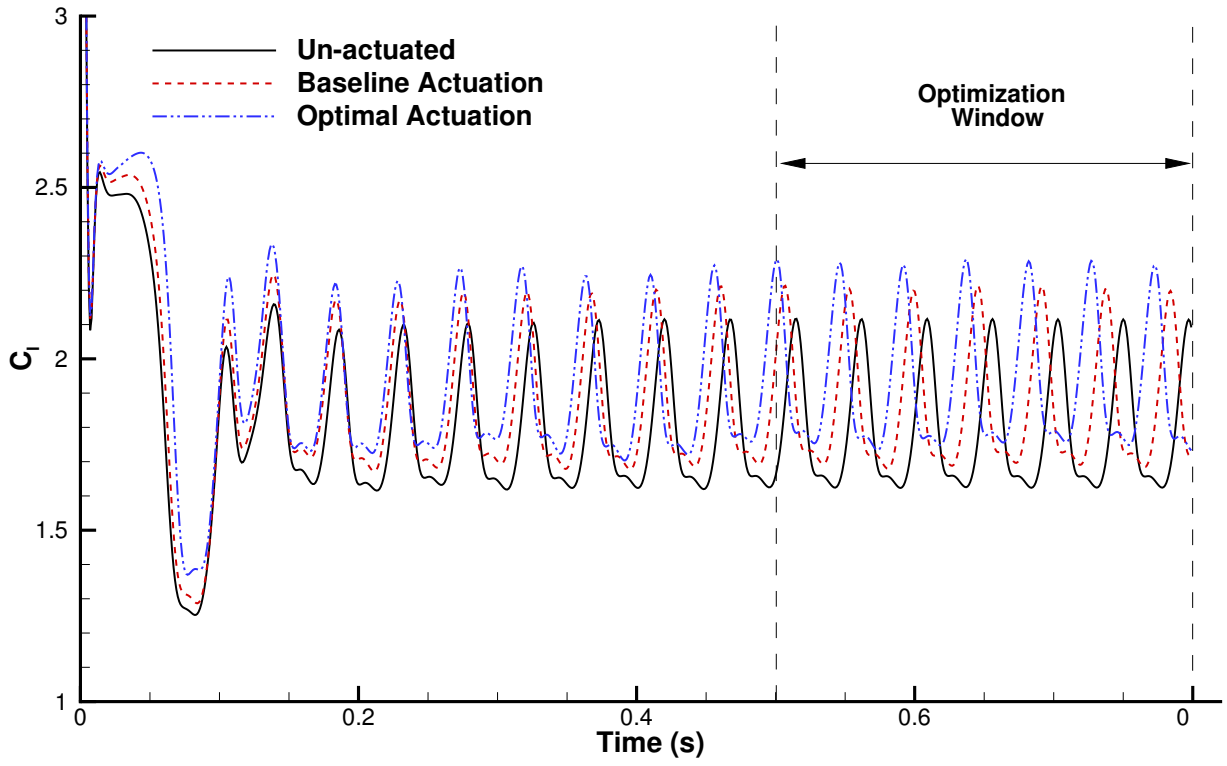

Figure 5: Time history of lift coefficient over 800 time iterations for the un-actuated (slits-coverd), baseline actuated and optimally actuated cases

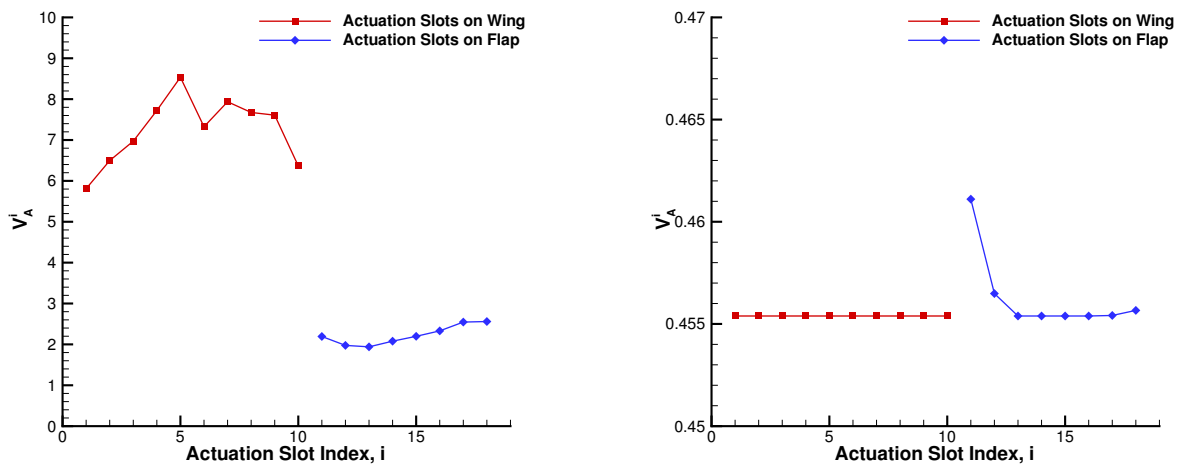

(a) Lift Maximized

(b) Noise Minimized

Figure 6: Optimal actuation velocity magnitude V_A^i of the lift-maximized (a) and noise-minimized case (b) at the 18 actuation slots on the wing and flap suction side

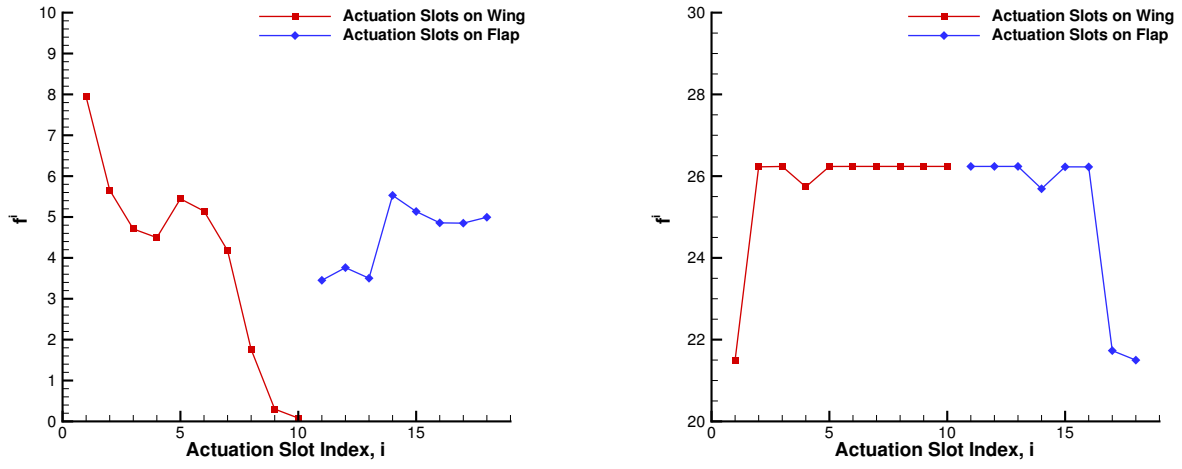

(a) Lift Maximized

(b) Noise Minimized

Figure 7: Optimal actuation frequency f^i of the lift-maximized (a) and noise-minimized case (b) at the 18 actuation slots on the wing and flap suction side

	NLR7301	Lift Maximized	Noise Minimized
J_L	1.8735	1.9283	1.8471
J_N	2.3989×10^{-3}	2.6475×10^{-3}	2.3634×10^{-3}

Table 3: Performance comparison between lift maximization and noise minimization results

4 Conclusion and Future Work

We have developed an AD-based discrete adjoint framework to perform active flow control in order to reduce both flow separation and far-field noise. The resultant unsteady control sensitivities of a periodically blowing

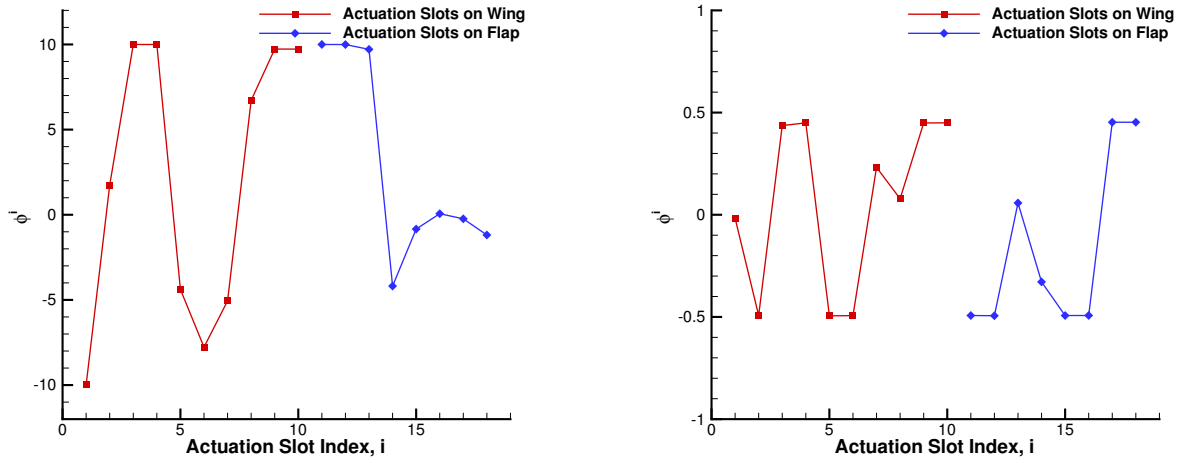

(a) Lift Maximized

(b) Noise Minimized

Figure 8: Optimal actuation phase shift ϕ^i of the lift-maximized (a) and noise-minimized case (b) at the 18 actuation slots on the wing and flap suction side

actuator with respect to both aerodynamic and aeroacoustic design objectives have been shown to be highly accurate using the canonical test case of a cylinder undergoing laminar vortex shedding. We are ready to perform optimal flow control on more challenging configurations.

The active flow control framework is applied to a NRL7301 wing-flap geometry for both lift maximization and noise minimization. The results show that significant lift augmentation can be achieved by optimally actuating the flow. In addition, the aerodynamic and aeroacoustic design objectives are shown to be competing in that a noise-minimized set of actuation parameters lead to an unacceptable loss of lift and vice versa.

As the next step, we plan to present a hybrid shape-AFC optimization on a droop nose airfoil with a high flap deflection. Lift enhancement and noise suppression will be achieved via shape optimization of the main airfoil body including the droop nose and optimal flow control on the flap suction side.

One shortcoming of AFC, among others, is its energy expenditure – auxiliary energy input is required to actuate the flow. In the near future, this will be addressed by adding an optimization constraint accounting for the actuation energy as suggested by Wassen and Thiele [11]

References

[1] M. Gad el Hak. *Flow Control, Passive Active Reactive Flow Management*. Cambridge University Press, 2000.

[2] A. Nemil, E. Özkaya, N.R. Gauger, F. Kramer, T. Höll, and F. Thiele. Optimal design of active flow control for a complex high-lift configuration. *AIAA 2014-2515*, 2014.

[3] T. D. Economon, F. Palacios, S.R. Copeland, T.W. Lukaczyk, and J.J. Alonso. Su2: An open-source suite for multiphysics simulation and design. *AIAA Journal*, 2015.

[4] B. Y. Zhou, T. Albring, N. R. Gauger, C. R. Ilario da Silva, T. D. Economon, and J. J. Alonso. An efficient unsteady aerodynamic and aeroacoustic design framework using discrete adjoint. *AIAA 2016-3369*, 2016.

[5] T. Colonius and S. K. Lele. Computational aeroacoustics: progress on nonlinear problems of sound generation. *Progress in Aerospace Sciences*, 40:345–416, 2004.

[6] D. P. Lockard. An efficient, two-dimensional implementation of the ffowcs williams and hawkings equationn. *Journal of Sound and Vibration*, 4:897–911, 2000.

[7] E. J. Nielsen and W. T. Jones. Integrated design of an active flow control system using a time-dependent adjoint method. *Math. Model. Nat. Phenom.*, 6(3):141–165, 2012.
[8] A. Griewank and A. Walther. *Evaluating Derivatives: Principles and Techniques of Algorithmic Differentiation*. Other Titles in Applied Mathematics, SIAM, 2008.
[9] R. Hogan. Fast reverse-mode automatic differentiation using expression templates in c++. *Transactions on Mathematical Software*, 26:1–16, 2014.
[10] T. A. Albring, M. Sagebaum, and N. R. Gauger. Efficient aerodynamic design using the discrete adjoint method in su2. *AIAA 2016-3518*, 2016.
[11] E. Wassen and F. Thiele. Simulation of active separation control on a generic vehicle. *AIAA 2010-4702*.